Title

LIGHT-DEFLECTION ERRORS IN THE INTERFEROMETRY OF ELECTROCHEMICAL MASS TRANSFER BOUNDARY LAYERS

Authors

McLarnon, F.R.
Muller, R.H.
Tobias, C.W.

Publication Date

1974-03-01

Submitted to the Journal of the
Electrochemical Society

LBL-2240
Preprint

LIGHT-DEFLECTION ERRORS IN THE INTERFEROMETRY OF ELECTROCHEMICAL MASS TRANSFER BOUNDARY LAYERS

F. R. McLarnon, R. H. Muller and C. W. Tobias

March 1974

Prepared for the U. S. Atomic Energy Commission
under Contract W-7405-ENG-48

LBL-2240

DISCLAIMER

LBL-2240

LIGHT-DEFLECTION ERRORS IN THE INTERFEROMETRY OF ELECTROCHEMICAL MASS TRANSFER BOUNDARY LAYERS

F. R. McLarnon, R. H. Muller and C. W. Tobias

Inorganic Materials Research Division, Lawrence Berkeley Laboratory and Department of Chemical Engineering; University of California Berkeley, California 94720

ABSTRACT

The effect of light-deflection on interferograms of electrochemical mass transfer boundary layers can result in substantial errors if interferograms are interpreted in the conventional way. Corrections in boundary layer thickness, interfacial concentration and interfacial concentration gradient for the convection-free electrodeposition of Cu from aqueous $CuSO_4$ have been correlated to provide estimates for a wide range of experimental conditions.

Key Words

Interferometry; Refraction; Diffusion; Mass Transfer

INTRODUCTION

Concentration profiles of single solutes in electrolytes near working electrodes can, in principle, be quantitatively observed by interferometric techniques. Such observations are useful in the study of transport processes and in the analysis of different measures designed to provide uniform accessibility and increased reaction rates at electrodes. Some of the advantages of interferometry compared to other means of observing boundary layers and local transport rates are high resolution for concentration changes (typically 10^{-5} M) and the possibility for continuous observation without disturbance (e.g., of flow), not restricted to conditions of limiting current.

In the conventional interpretation of interferograms, local changes in the phase depicted by the interferogram are taken as a direct measure of local refractive index variations in the object. Such an interpretation is often not valid because it assumes that light travels along a straight line through the specimen. Refractive index variations normal to the propagation direction of a light beam produce a deflection of the beam (refraction, Schlieren effect) that results in two types of distortions in the interferograms: a) Geometrical distortion due to displacement of the beam normal to its propagation direction. This effect falsifies conventional interpretation of distance on the interferogram and causes displacement of the apparent electrode/electrolyte interface. b) Phase distortion due to increased geometrical path length and passage of the beam through regions of varying refractive-index. Quantitative concentration profiles

therefore often cannot be derived by the conventional interpretation of interferograms.

Details of computational techniques, that have been developed to account for the effect of light-deflection on interferograms of one-dimensional boundary layers, have been described elsewhere.[1,2] Suffice it to say that for any concentration profile, the shapes of (double beam) interference fringes can now be calculated taking into account effects of light deflection. It has been found that distortions in the interferogram depend strongly on the position of the plane of focus of the imaging objective. Although for each concentration profile a plane of focus can be found[3] for which the location of the electrode surface is not distorted on the interferogram, for the observation of cathodic boundary layers (to be considered here) it is preferable[2] to focus on the inside of the cell wall on the light-entrance side of the cell, where suitable targets can be inscribed. (For anodic boundary layers, it would be preferable to focus on the inside of the cell wall on the light-exit side.)

It is the purpose of this paper to present correlations of light-deflection errors for the interferometric observation of boundary layers so that investigators may estimate errors to be expected under a wide range of experimental conditions.

LIGHT-DEFLECTION ERRORS

Figure 1 shows the experimental interferogram of a concentration boundary layer. Superimposed are the theoretical concentration profile, AE, derived by use of the Sand[4] equation and an interference fringe, BF, computed from the concentration profile by taking light-deflection effects into account.

The ordinate on Fig. 1 denotes distance from the true (undistorted) image of the electrode surface. Local changes in the phase of transmitted light, visible as displacements of originally straight interference fringes, have been related to local concentration changes, as shown on the abscissa. The relationship has been based on the conventional interpretation of interferograms that assumes straight-line light propagation. Thus, local changes in phase have been linearly related to changes in concentration (or refractive index) at the corresponding point in the image.

If the interferogram was free of light-deflection errors, the interference fringes would follow the theoretical concentration profile AE. The figure illustrates that the apparent location of the interface on the interferogram has receeded from its original position, identified by $y = 0$. Also, the apparent concentration change over the boundary layer is smaller than the true change.

Conventional interpretation of the interferogram in Fig. 1 would therefore lead to a boundary layer thickness that is too large. If we define the extent of the boundary layer as the region containing 90% of the concentration variation, the error e_t in boundary layer thickness can be defined as a difference in ordinates of points B, E and F

$$e_t = y|_F - y|_B - y|_E \ .$$

Similarly, the apparent interfacial concentration is too high and the error can be formulated as a difference of abscissas

$$e_c = C|_B - C|_A \ .$$

The interfacial concentration (refractive index) gradient is too low. The error can be represented by the difference in slope of the two curves at the interface

$$e_g = \left.\frac{dC}{dy}\right|_B - \left.\frac{dC}{dy}\right|_A \ .$$

In addition to the above <u>absolute</u> errors in the interferometry of boundary layers, it is often desireable to estimate the <u>relative</u> errors. Such relative errors in boundary layer thickness, interfacial concentration and interfacial concentration gradient, as shown in Figs. 8-13, are defined here as

$$\varepsilon_t = \frac{e_t}{y|_E}$$

$$\varepsilon_C = \frac{e_c}{C_b - C|_A}$$

$$\varepsilon_g = \frac{e_g}{\left.\frac{dC}{dy}\right|_A} \ .$$

CONVECTION-FREE BOUNDARY LAYERS

Diffusion boundary layers free of convection effects offer a good model for optical investigation since the concentration profiles are easily derived, and experimental results can serve to test the optical calculations. Convention-free transport conditions are common in electrochemical studies, and the results can be used as a basis for convective transport studies. Figure 2 shows the similarity between interferometric errors seen in boundary layers with and without convection.

The convectionless electrodeposition of a metal cation from a stagnant layer of an aqueous binary salt electrolyte is described by the unsteady-state diffusion equation in one dimension

$$\frac{\partial C}{\partial t} = D \frac{\partial^2 C}{\partial y^2} . \qquad (1)$$

The current density is related to the interfacial concentration gradient by

$$i = \frac{zFD}{1-t_+} \left.\frac{\partial C}{\partial y}\right|_{y=0} . \qquad (2)$$

---

*Concentration-independent diffusivity will be assumed. Solutions for variable diffusivity can also be obtained, although not in a convenient closed form.

For potentiostatic electrodeposition, the boundary conditions are

$$C = C_s \quad \text{at} \quad y = 0 \, , \; t > 0 \tag{3}$$

$$C = C_b \quad \text{at} \quad t = 0 \, , \; \text{all} \; \; y \tag{4}$$

$$C = C_b \quad \text{as} \quad y \to \infty \, . \tag{5}$$

The solution, first obtained by Cottrell,[5] is

$$\theta = \text{erf} \; \zeta \tag{6}$$

$$i = \frac{zF(\Delta C)}{1-t_+} \sqrt{\frac{D}{\pi t}} \tag{7}$$

where $\text{erf} \; \zeta$ is the error function of dimensionless distance

$$\zeta = \frac{y}{2\sqrt{Dt}} \, , \tag{8}$$

$\Delta C = C_b - C_s$ and the dimensionless concentration

$$\theta = \frac{C - C_s}{\Delta C} \, . \tag{9}$$

For galvanostatic electrodeposition, the boundary conditions to Eq. (1) are:

$$\frac{\partial C}{\partial y} = \text{constant at} \quad y = 0 \, , \; t > 0 \tag{10}$$

$$C = C_b \quad \text{at} \quad t = 0 \, , \; \text{all} \; \; y \tag{11}$$

$$C = C_b \quad \text{as} \quad y \to \infty \, .$$

The solution, first obtained by Sand,[4] is

$$\theta = 1 + \sqrt{\pi}\,\zeta(1 - \text{erf}\,\zeta) - e^{-\zeta^2} \tag{13}$$

$$\Delta C = \frac{2i\,(1 - t_+)}{zF}\sqrt{\frac{t}{\pi D}} \tag{14}$$

Concentration profiles are now calculated for the two types of convectionless boundary layers, using electrodeposition of Cu from aqueous $CuSO_4$ as a model. $C_s = 0$ for all calculations, and $C_b = 0.01$, 0.1 or 0.2M $CuSO_4$ ($\Delta C = 0.01$, 0.1 or 0.2). For constant potential calculations, time t is varied to give different concentration profiles and interfacial mass flux rates. For constant current calculations, various current densities are used (substituting Eq. (2) into Eq. (10)) to give different concentration profiles and interfacial mass flux rates. Note that specification of i and ΔC fixes t through Eq. (14). A diffusion coefficient[6] $D = 6\times10^{-6}$ cm^2/sec and Cu^{++} transference number[7] $t_+ = 0.36$ (typical values for 0.1M $CuSO_4$ at 25°C) are used in all calculations. Representative concentration profiles employed in the optical analysis are shown in Figs. 3 and 4.

ERROR CALCULATIONS

Cell dimensions and optical constants must be specified in order to compute interferograms for concentration profiles. The electrode, which fully occupies the space between the glass sidewalls, was assigned widths of 1.0, 2.5, 5.0, 10.0 and 20.0 mm. In order to simulate our experimental cell, the glass sidewalls were assumed to be 12.7 mm wide with a refractive-index of 1.5231. However, refraction in the glass sidewalls has a negligible effect on light-deflection errors.[3] Light of 632.8 nm wavelength is assumed incident parallel to the planar electrode surface and perpendicular to the glass sidewalls. The plane of focus is chosen as the plane where light enters the electrolyte. Electrolyte refractive-index was experimentally found to be a linear function of $CuSO_4$ concentration at 632.8 nm wavelength and 25°C:

$$n = 1.3311 + 0.029\ C \qquad (15)$$

Interferograms similar to the dashed line in Fig. 1 are now calculated from concentration profiles using the above-mentioned computational technique.[1]

Absolute errors in boundary layer thickness, interfacial concentration and interfacial concentration gradient are shown in Figs. 5, 6 and 7, respectively for a 10 mm wide electrode. Current density (interfacial refractive-index gradient) was chosen as abscissa because it is an easily measured variable. Note that a positive error means that the value of a variable on the interferogram is larger than the true value.

Relative errors in boundary layer thickness, interfacial concentration and interfacial concentration gradient are shown in Figs. 8-10. These figures also demonstrate the dependence of errors on concentration difference ΔC. The effect of electrode width is described in Figs. 11-13.

DISCUSSION

Figures 5, 6 and 7 show that for a 10 mm wide electrode, the light-deflection errors depend strongly on current density and concentration difference ΔC but weakly on the specific boundary condition (potentiostatic or galvanostatic). For current densities in the order of a mA/cm^2, the errors are independent of ΔC and boundary condition. In this region of current densities, the error in boundary layer thickness shows a linear dependence on current density and a quadratic dependence on electrode width.[8] Above about 7 mA/cm^2 for $\Delta C = 0.1$ and about 10 mA/cm^2 for $\Delta C = 0.2$, the light rays entering the boundary layer at the electrode surface are deflected so much that they leave the boundary layer before they leave the electrolyte. This effect shows up as an error extremum in Figs. 5 and 6 and as an inflection point in Fig. 7. As infinite current density is approached, the error in boundary layer thickness approaches zero, the error in interfacial concentration approaches ΔC and the error in interfacial concentration gradient approaches negative infinity.

The trend toward apparent negative concentrations (i.e., on the interferogram) seen in Figs. 6, 9 and 12 is an artifact caused by the choice of focal plane position. For focus in the center of the cell, for instance, no such negative errors would occur.

Figures 8-10 show that relative errors are smaller for larger concentration difference ΔC. However, for large concentration differences, interferogram interpretation can be impeded by crowding of the fringes near the interface.

Figures 11-13 show that similar to absolute errors derived analytically for constant concentration gradients of unlimited extent[3] relative errors strongly decrease with decreasing cell width, but are negligible only for electrodes thinner than a few mm.

CONCLUSIONS

Light deflection effects in the interferometry of electrochemical mass transfer boundary layers can lead to serious errors in the derivation of concentration profiles unless appropriate corrections in the interpretation of interferograms are employed. The magnitude of such errors may be estimated from the data presented in Figs. 5-13, but the accurate interpretation of interferograms with significant light-deflection effects requires individual optical analysis.[2] Light-deflection errors are small (<10%) for small current densities (below 2.5 mA/cm^2 for a 1 cm wide electrode) or narrow electrodes (less than 2.5 mm for up to 10 mA/cm^2).

ACKNOWLEDGEMENTS

This work was conducted under the auspices of the U. S. Atomic Energy Commission.

REFERENCES

1. K. W. Beach, R. H. Muller and C. W. Tobias, J. Opt. Soc. Am. 63, 559 (1973).

2. K. W. Beach, Optical Methods for the Study of Convective Mass Transfer Boundary Layers on Extended Electrodes (Ph.D. Thesis), UCRL-20324, July 1971.

3. R. H. Muller in Advances in Electrochemistry and Electrochemical Engineering, R. H. Muller, ed. (Wiley-Interscience, New York, 1973), Vol. 9, pp. 326-353.

4. H. J. S. Sand, Phil Mag. (6) 1, 45 (1901).

5. F. G. Cottrell, Z. Physikal. Chem. 42, 385 (1903).

6. W. G. Eversole, H. M. Kindsvater and J. D. Peterson, J. Phys. Chem. 46, 370 (1942)

7. J. J. Fritz and C. R. Fuget, J. Phys. Chem. 62, 303 (1958).

8. F. R. McLarnon (to be published).

NOMENCLATURE

C	concentration [mole/liter]
C_b	bulk concentration [mole/liter]
C_s	interfacial concentration [mole/liter]
D	diffusion coefficient [cm^2/sec]
e_t	error in boundary layer thickness [mm]
e_c	error in interfacial concentration [M $CuSO_4$]
e_g	error in interfacial concentration gradient [M $CuSO_4$ cm^{-1}]
F	Faraday constant [coul/equiv]
i	current density [A/cm^2]
n	refractive-index
t	time after current (voltage) switch-on [s]
t_+	cation transference number
y	distance from electrode [mm]
z	cation valence
ΔC	$C_b - C_s$ [mole/liter]
ε_t	relative error in boundary layer thickness
ε_c	relative error in interfacial concentration
ε_g	relative error in interfacial concentration gradient
ζ	dimensionless distance (Eq. (8))
θ	dimensionless concentration (Eq. (9))

FIGURE CAPTIONS

Fig. 1. Experimental interferogram of a concentration boundary layer during galvanostatic deposition of copper on a 10 mm wide electrode. i = 10.0 mA/cm^2, C_b = 0.1M $CuSO_4$ and t = 10.0 s.

——— Theroretical concentration profile AE corresponding to experimental conditions (calculated from Eq. (13)).

----- Computed interference fringe BF corresponding to theoretical concentration profile.

A True interfacial concentration and position.

B Apparent interfacial concentration and position.

E True (90%) boundary layer edge (position where θ = 0.9).

F Apparent boundary layer edge.

Fig. 2. Interferograms and concentration profiles for galvanostatic electrodeposition of Cu from 0.1M $CuSO_4$ at 10.0 mA/cm^2, t = 10.0 s.

• • • Experimental interferogram.

----- Concentration profile derived from the interferogram by an iterative technique.[1,8]

——— Interference fringe associated with derived concentration profile.

····· Theoretical concentration profile corresponding to experimental conditions (calculated from Eq. (13)).

A Convectionless boundary layer.

B Forced convection boundary layer, Re = 1000, 2.0 cm (1.4 hydraulic diameters) downstream from electrode leading edge.

Fig. 3. Concentration profiles for potentiostatic conditions.

——— ΔC = 0.1M $CuSO_4$

----- ΔC = 0.2M $CuSO_4$

a i = 10.0 mA/cm^2, t = 17.5 s

b i = 20.0, t = 4.4 s

c i = 30.0, t = 1.9 s

d i = 10.0, t = 70.0 s

e i = 20.0, t = 17.5 s

f i = 30.0, t = 7.8 s

Fig. 4. Concentration profiles for galvanostatic conditions. ΔC and i designation as in Fig. 3.

a t = 43.2 s

b t = 10.8 s

c t = 4.8 s

d t = 172.7 s

e t = 43.2 s

f t = 19.2 s

Fig. 5. Absolute error in boundary layer thickness. Electrode width = 10.0 mm.

——— potentiostatic boundary condition

------- galvanostatic boundary condition

a ΔC = 0.10 M $CuSO_4$

b ΔC = 0.20 M $CuSO_4$

Fig. 6. Absolute error in interfacial concentration. Designations as in Fig. 5.

Fig. 7. Absolute error in interfacial concentration gradient. Designations as in Fig. 5.

Fig. 8. Relative error in boundary layer thickness for various concentration differences. Electrode width = 10.0 mm, potentiostatic boundary condition.

a ΔC = 0.01 M $CuSO_4$

b ΔC = 0.10 M $CuSO_4$

c ΔC = 0.20 M $CuSO_4$

Fig. 9. Relative error in interfacial concentration for various concentration differences. Designations as in Fig. 8.

Fig. 10. Relative error in interfacial concentration gradient for various concentration differences. Designations as in Fig. 8.

Fig. 11. Relative error in boundary layer thickness for different electrode widths. ΔC = 0.1 M $CuSO_4$, potentiostatic boundary conditions.

a electrode width = 20.0 mm

b 10.0 mm

c 5.0 mm

d 2.5 mm

e 1.0 mm

Fig. 12. Relative error in interfacial concentration for different electrode widths. Designations as in Fig. 11.

Fig. 13. Relative error in interfacial concentration gradient for different electrode widths. Designations as in Fig. 11.

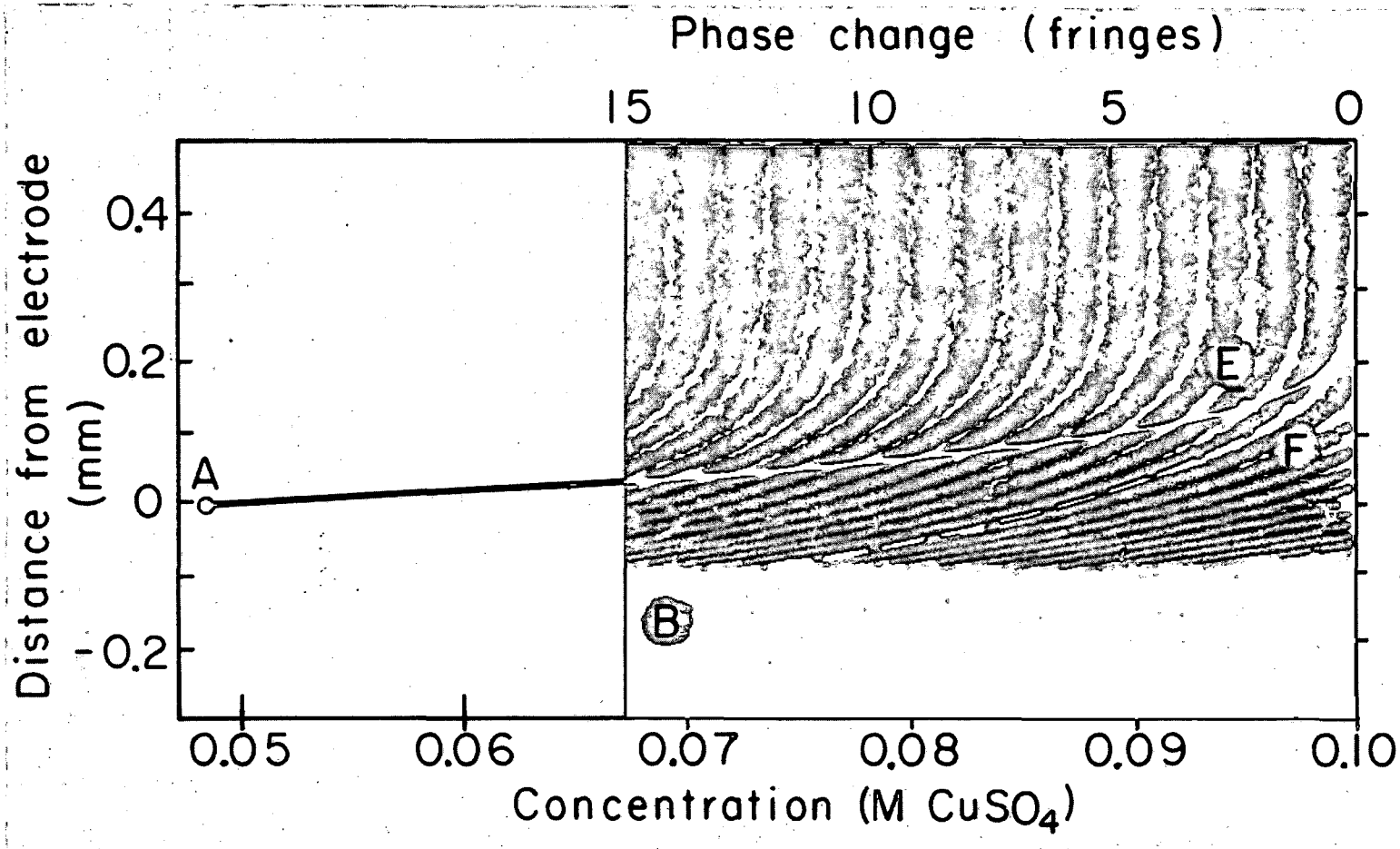
Phase change (fringes)
15
10
5
0
Distance from electrode (mm)
0.4
0.2
0
-0.2
A
B
E
F
0.05
0.06
0.07
0.08
0.09
0.10
Concentration (M CuSO4)
XBB 7311-6546

Fig. 1

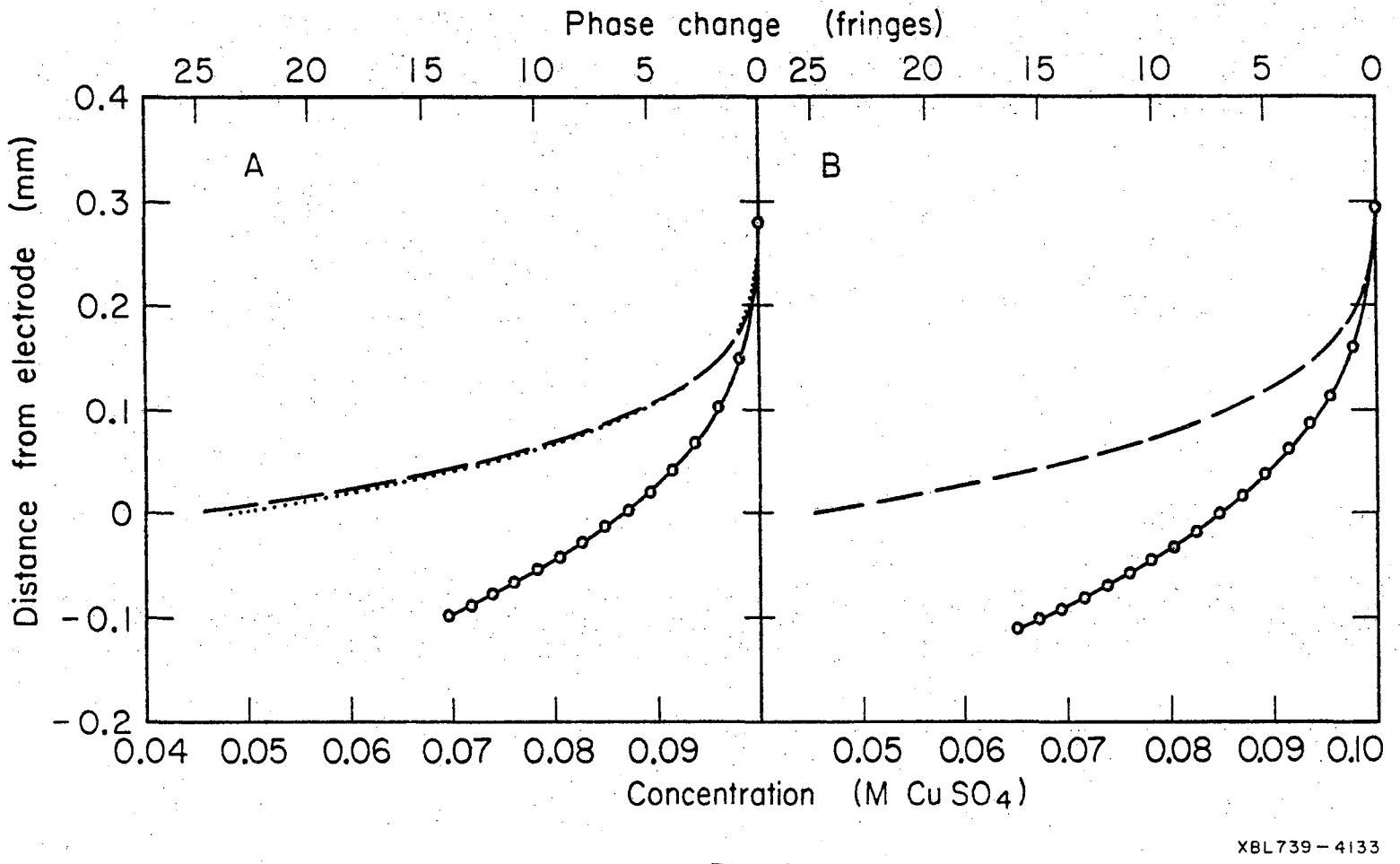

XBL739-4133

Fig. 2

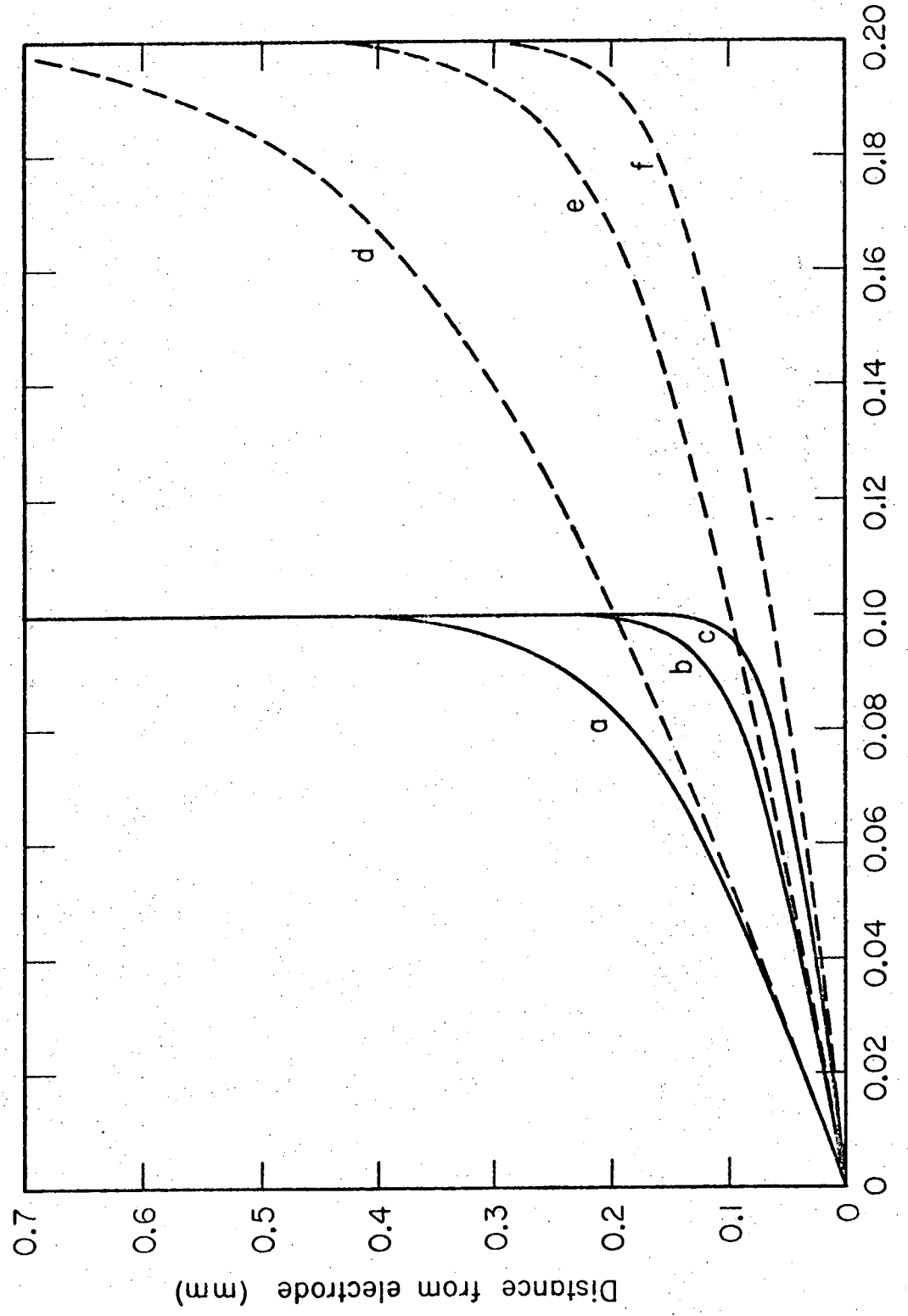

XBL 739-4134

Fig. 3

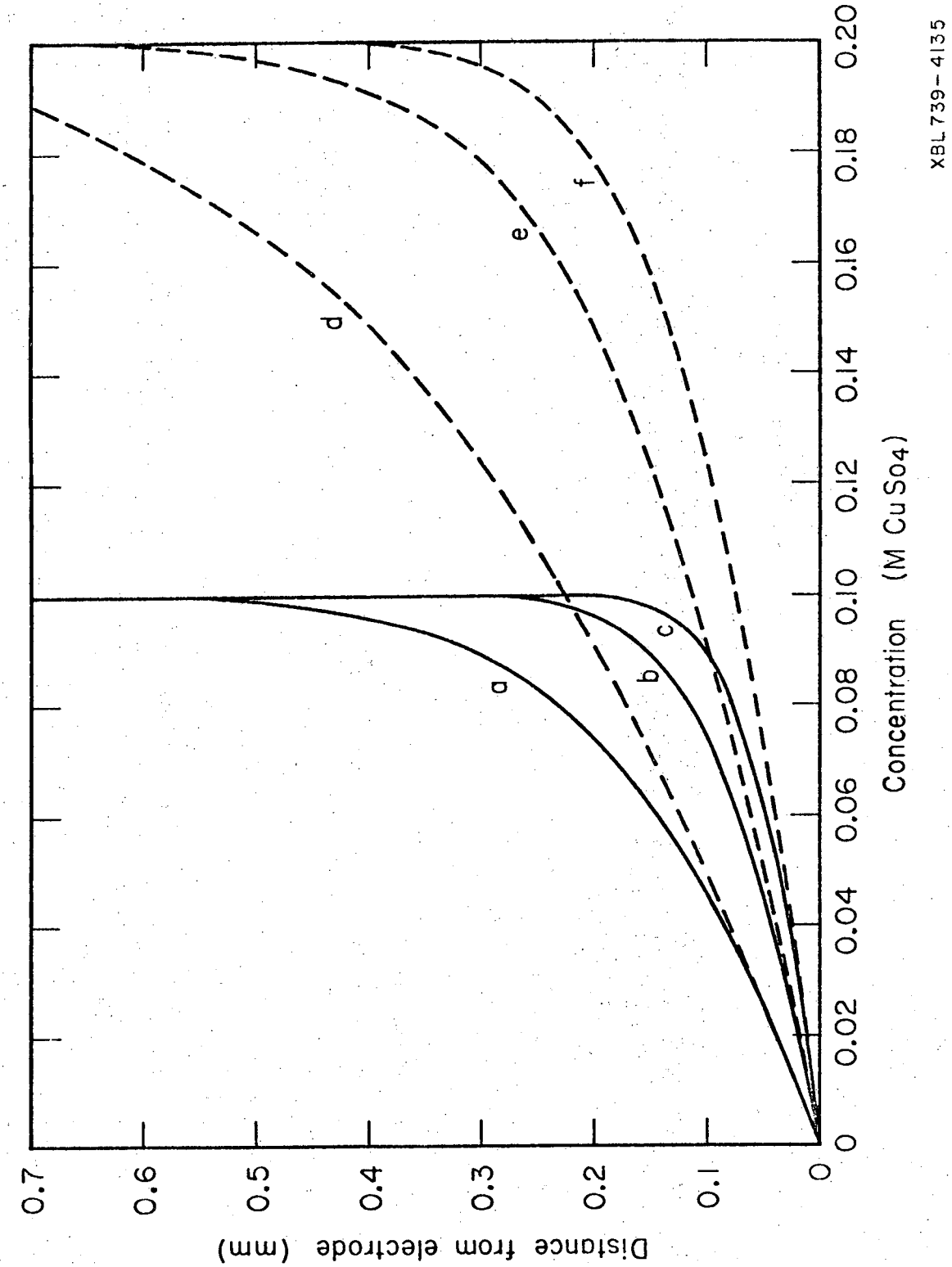

XBL 739-4135

Fig. 4

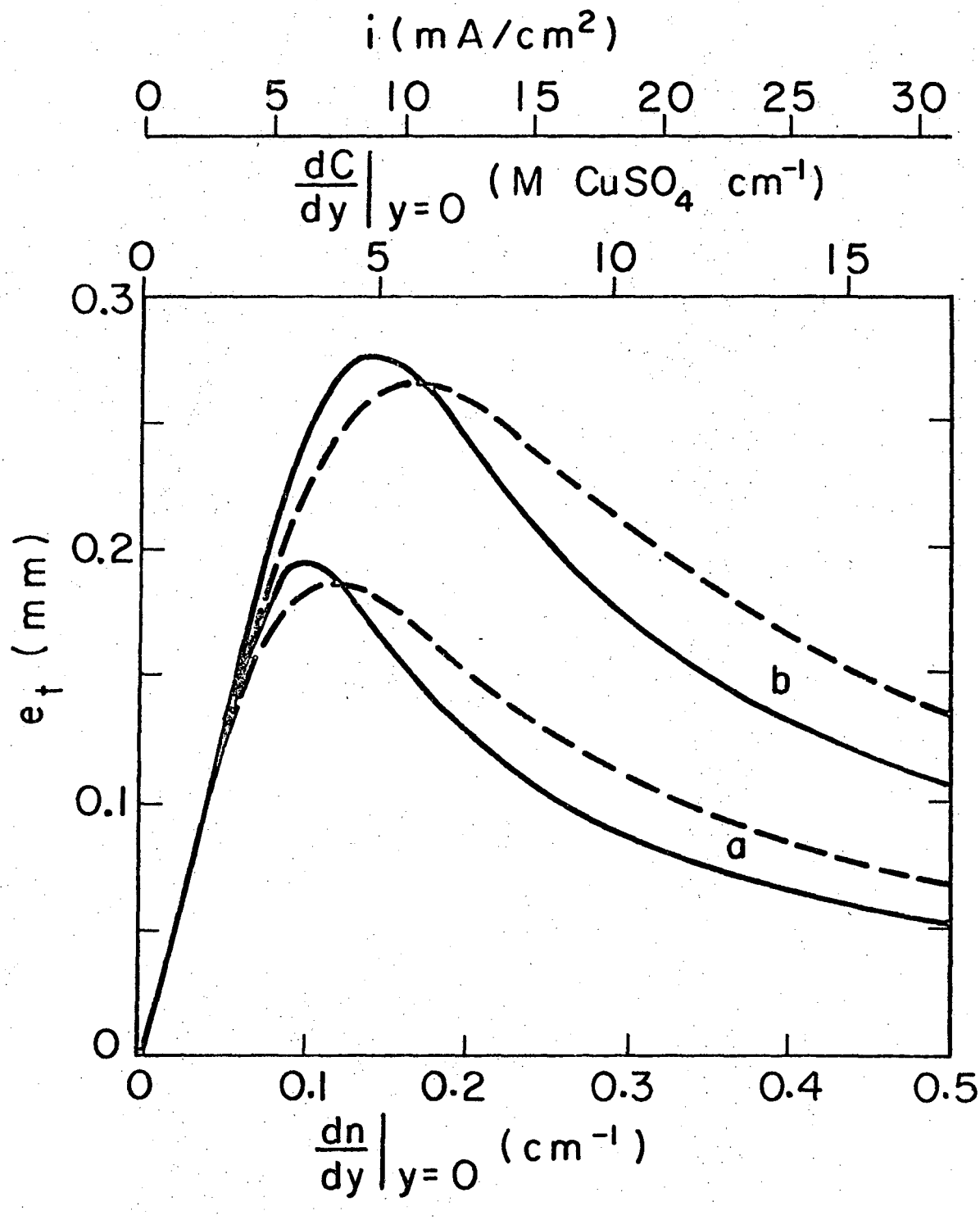

XBL741-2170

Fig. 5

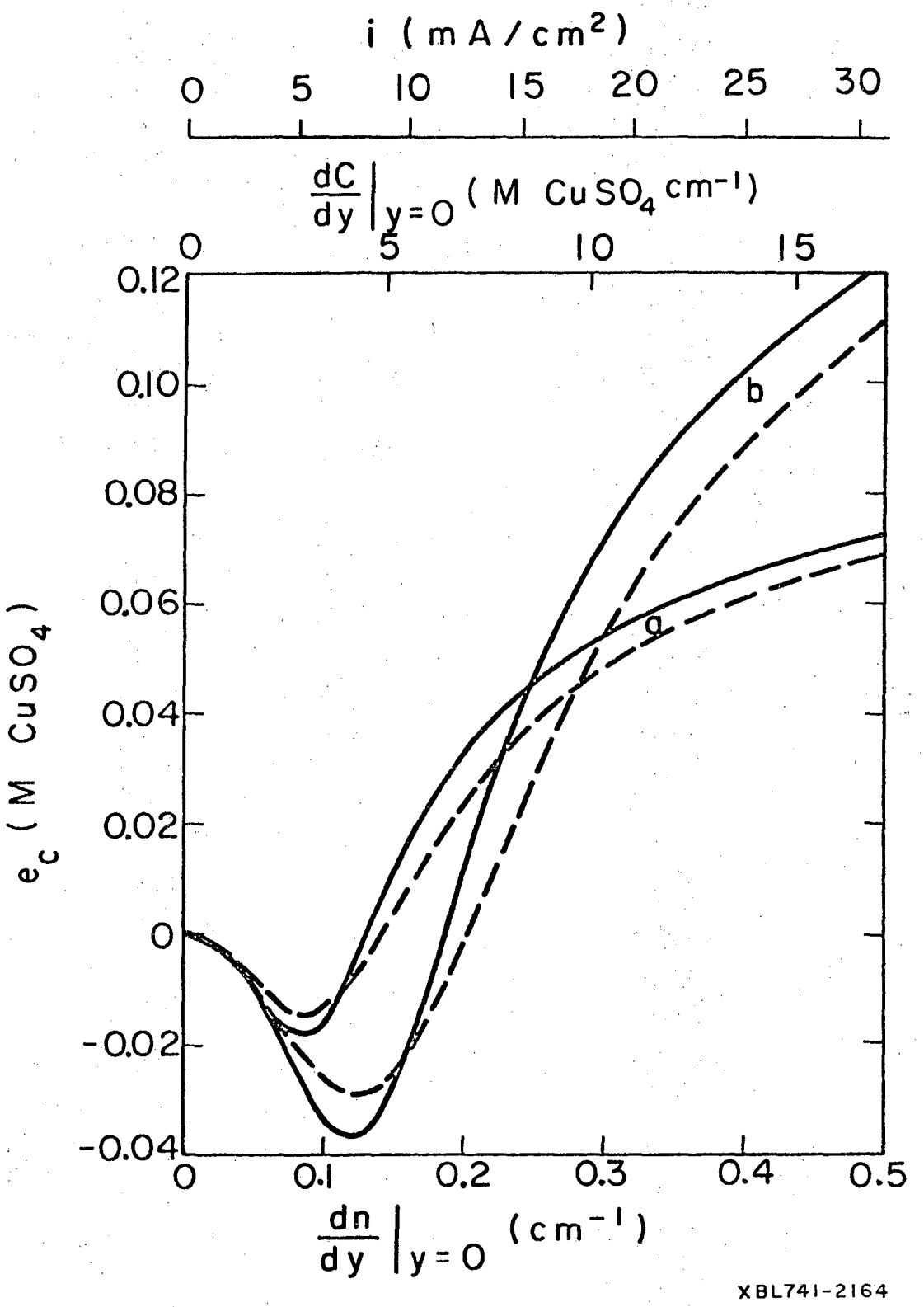
i (mA / cm²)
0
5
10
15
20
25
30
dC/dy |y=0 (M CuSO4 cm⁻¹)
0
5
10
15
0.12
0.10
0.08
0.06
0.04
0.02
0
-0.02
-0.04
e_c (M CuSO4)
b
a
0
0.1
0.2
0.3
0.4
0.5
dn/dy |y=0 (cm⁻¹)
XBL741-2164

Fig. 6

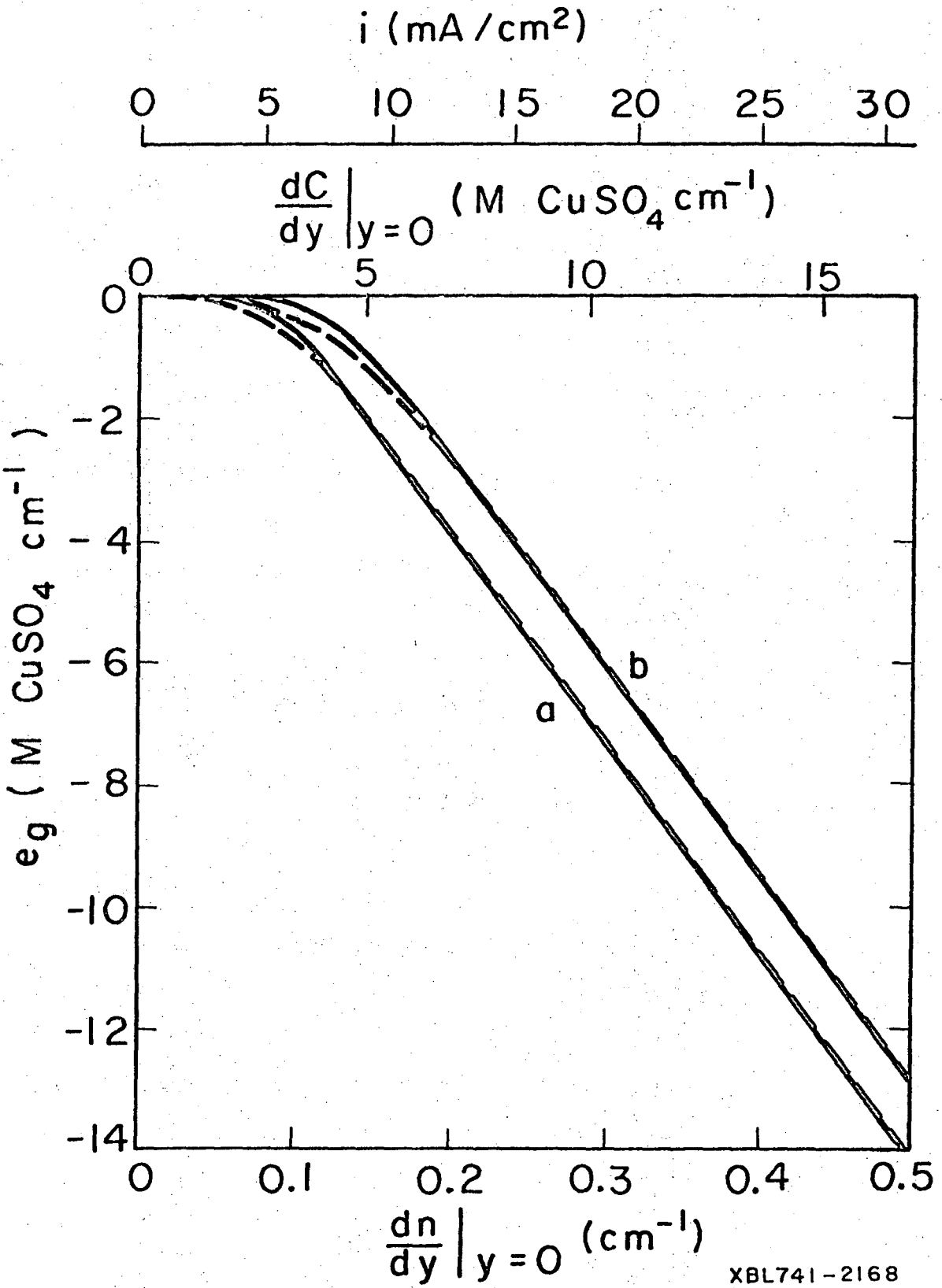
i (mA/cm²)
0
5
10
15
20
25
30
dC/dy |y=0 (M CuSO4 cm⁻¹)
0
5
10
15
eg (M CuSO4 cm⁻¹)
0
-2
-4
-6
-8
-10
-12
-14
a
b
0
0.1
0.2
0.3
0.4
0.5
dn/dy |y=0 (cm⁻¹)
XBL741-2168

Fig. 7

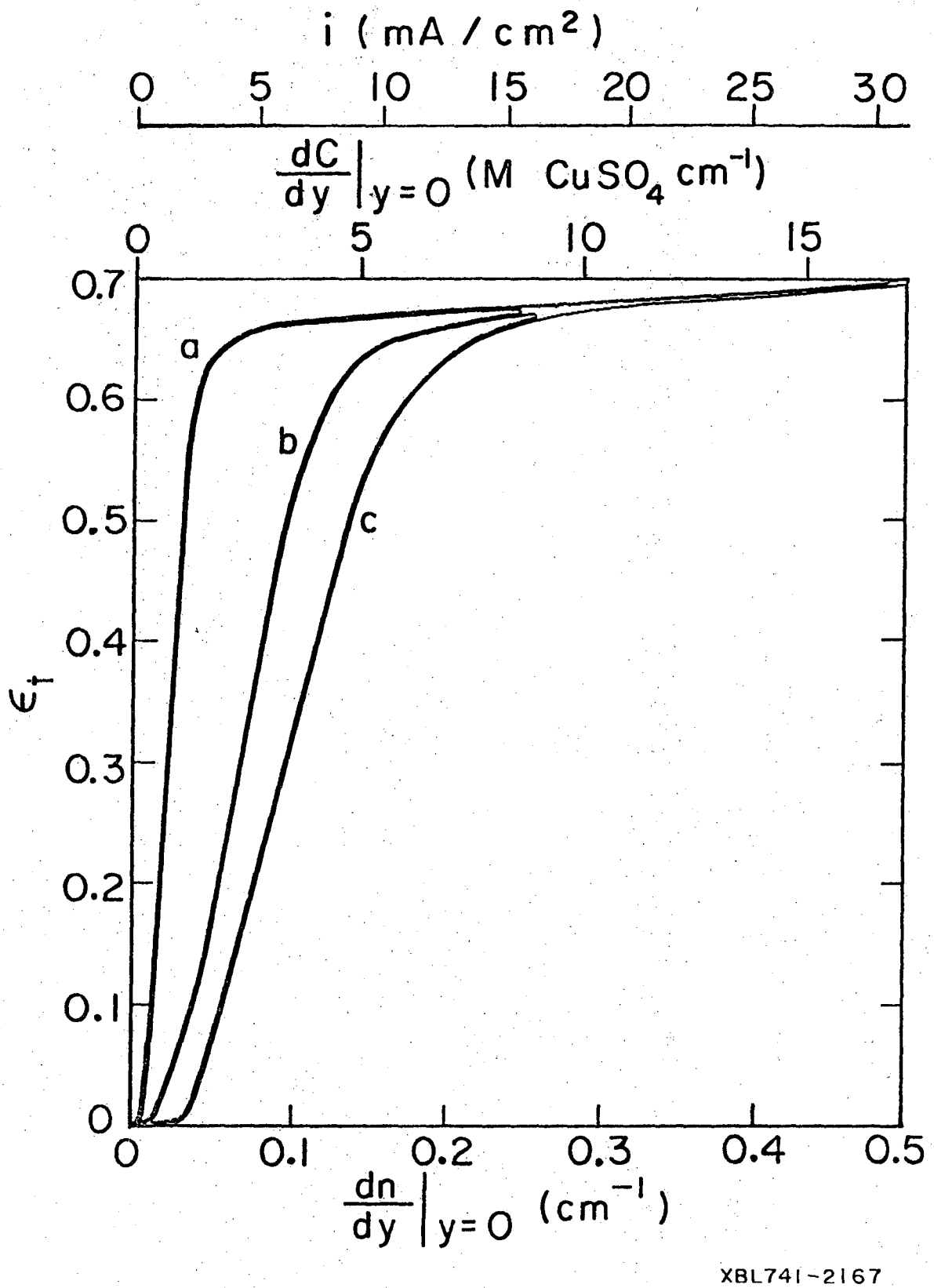
i (mA / cm²)
0
5
10
15
20
25
30
dC/dy |y=0 (M CuSO4 cm⁻¹)
0
5
10
15
0.7
0.6
0.5
0.4
0.3
0.2
0.1
0
ε+
a
b
c
0
0.1
0.2
0.3
0.4
0.5
dn/dy |y=0 (cm⁻¹)
XBL741-2167

Fig. 8

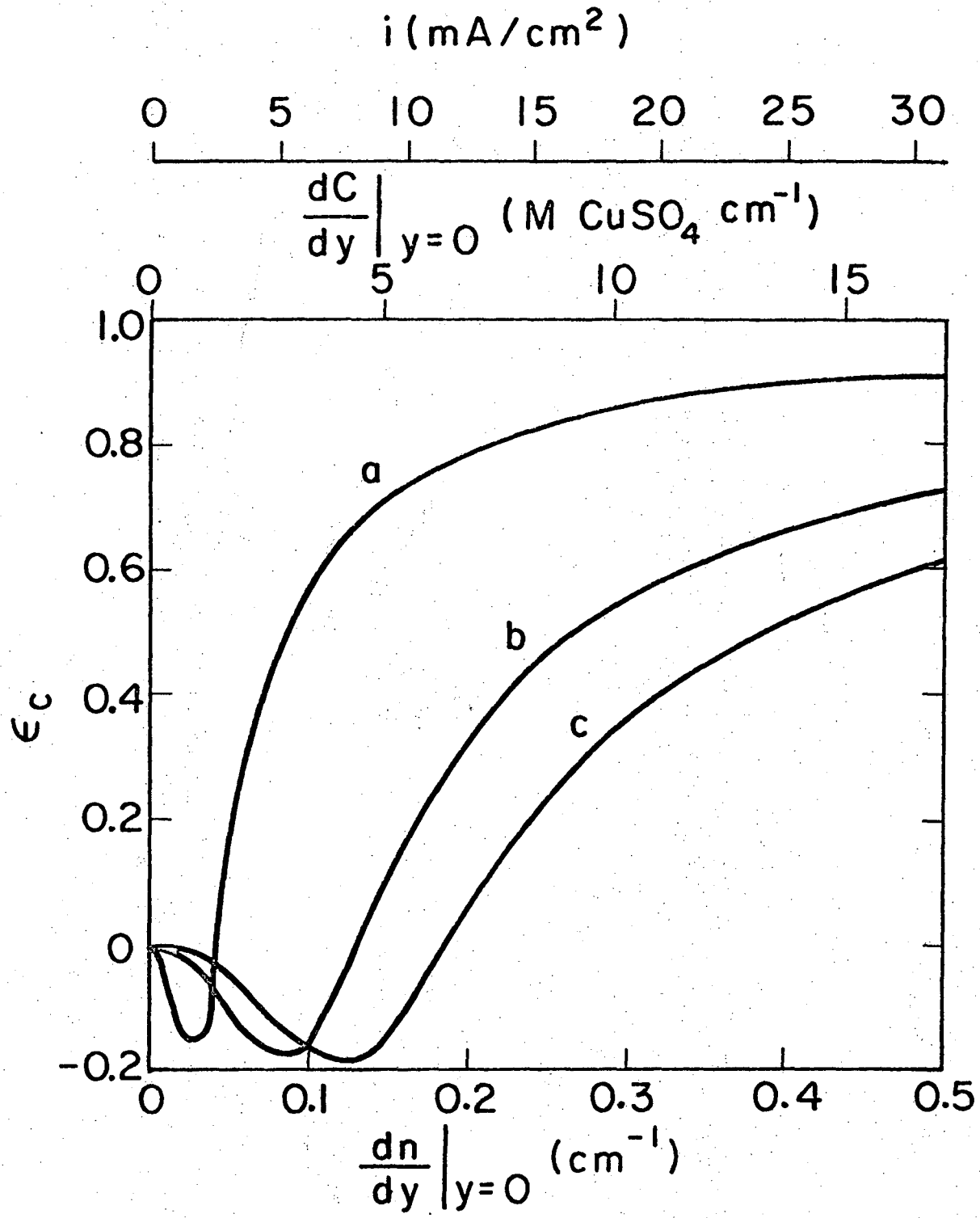
i (mA/cm²)
0
5
10
15
20
25
30
dC/dy | y=0 (M CuSO4 cm⁻¹)
0
5
10
15
1.0
0.8
0.6
0.4
0.2
0
-0.2
εc
a
b
c
0
0.1
0.2
0.3
0.4
0.5
dn/dy | y=0 (cm⁻¹)
XBL741-2166

Fig. 9

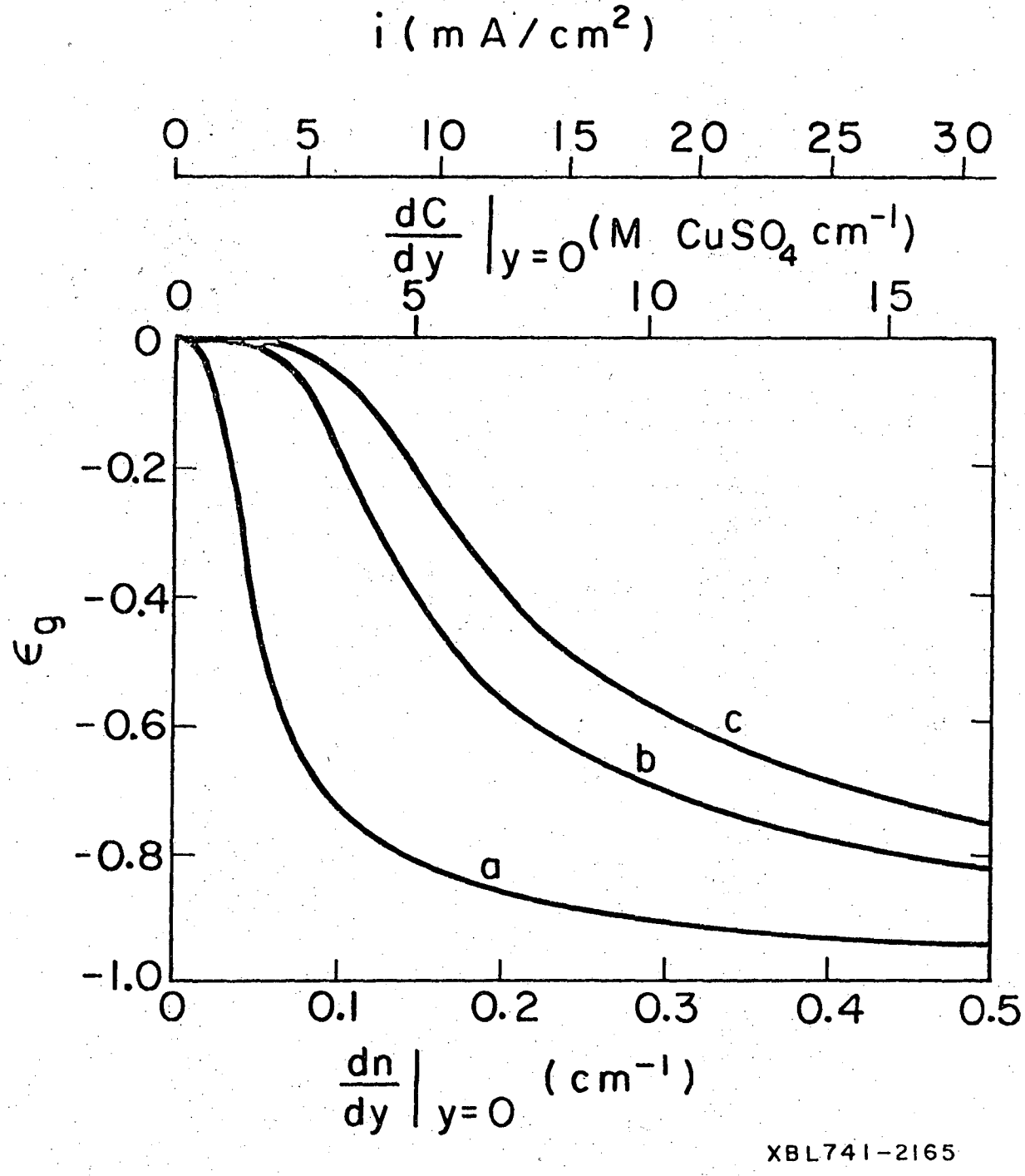
i (m A / cm²)
0
5
10
15
20
25
30
dC/dy |y=0 (M CuSO4 cm⁻¹)
0
5
10
15
0
-0.2
-0.4
-0.6
-0.8
-1.0
εg
a
b
c
0
0.1
0.2
0.3
0.4
0.5
dn/dy |y=0 (cm⁻¹)
XBL741-2165

Fig. 10

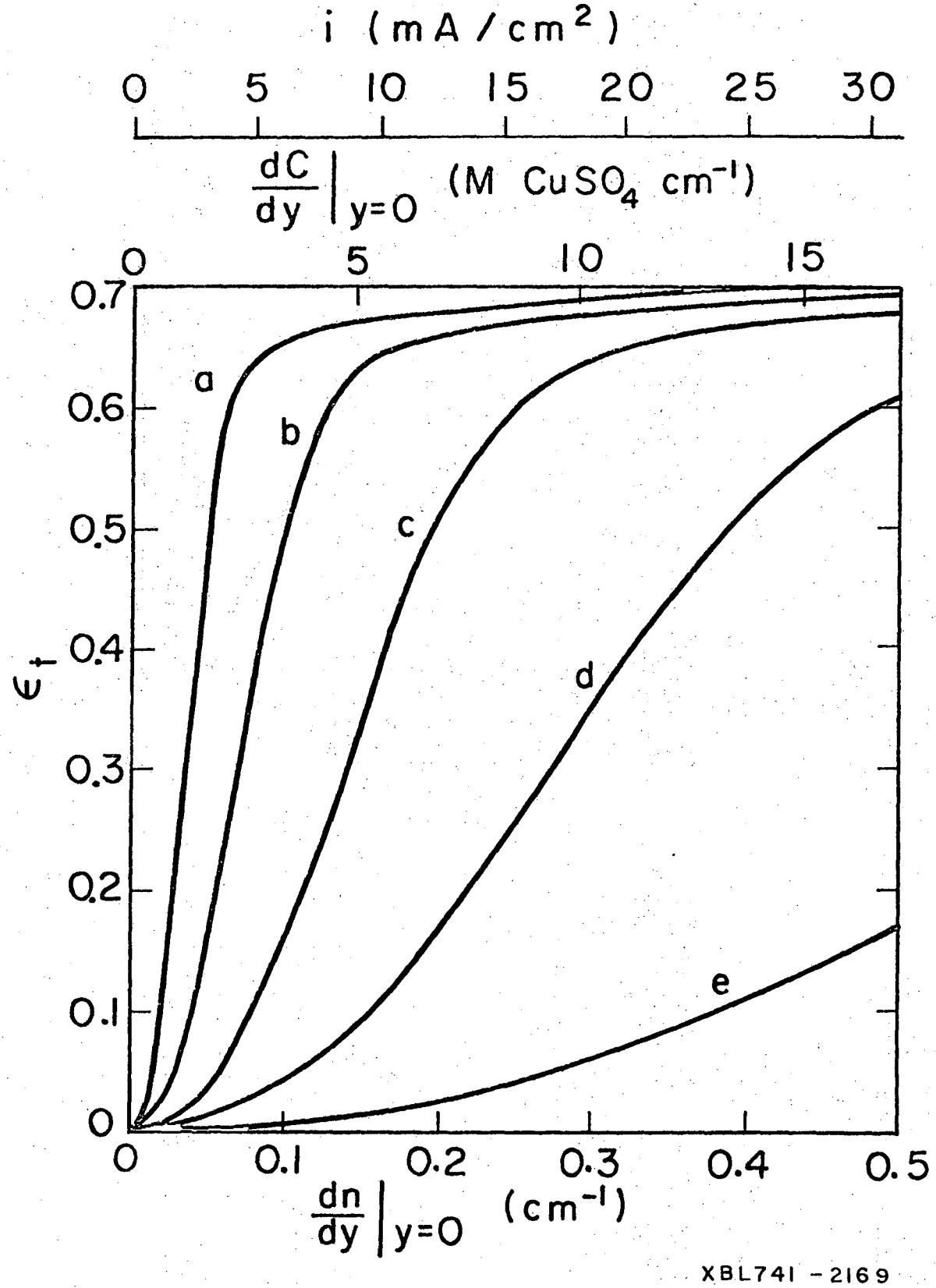
i (mA/cm²)
0
5
10
15
20
25
30
dC/dy | y=0 (M CuSO4 cm⁻¹)
0
5
10
15
0.7
0.6
0.5
0.4
0.3
0.2
0.1
0
ϵ_t
a
b
c
d
e
0
0.1
0.2
0.3
0.4
0.5
dn/dy | y=0 (cm⁻¹)
XBL741-2169

Fig. 11

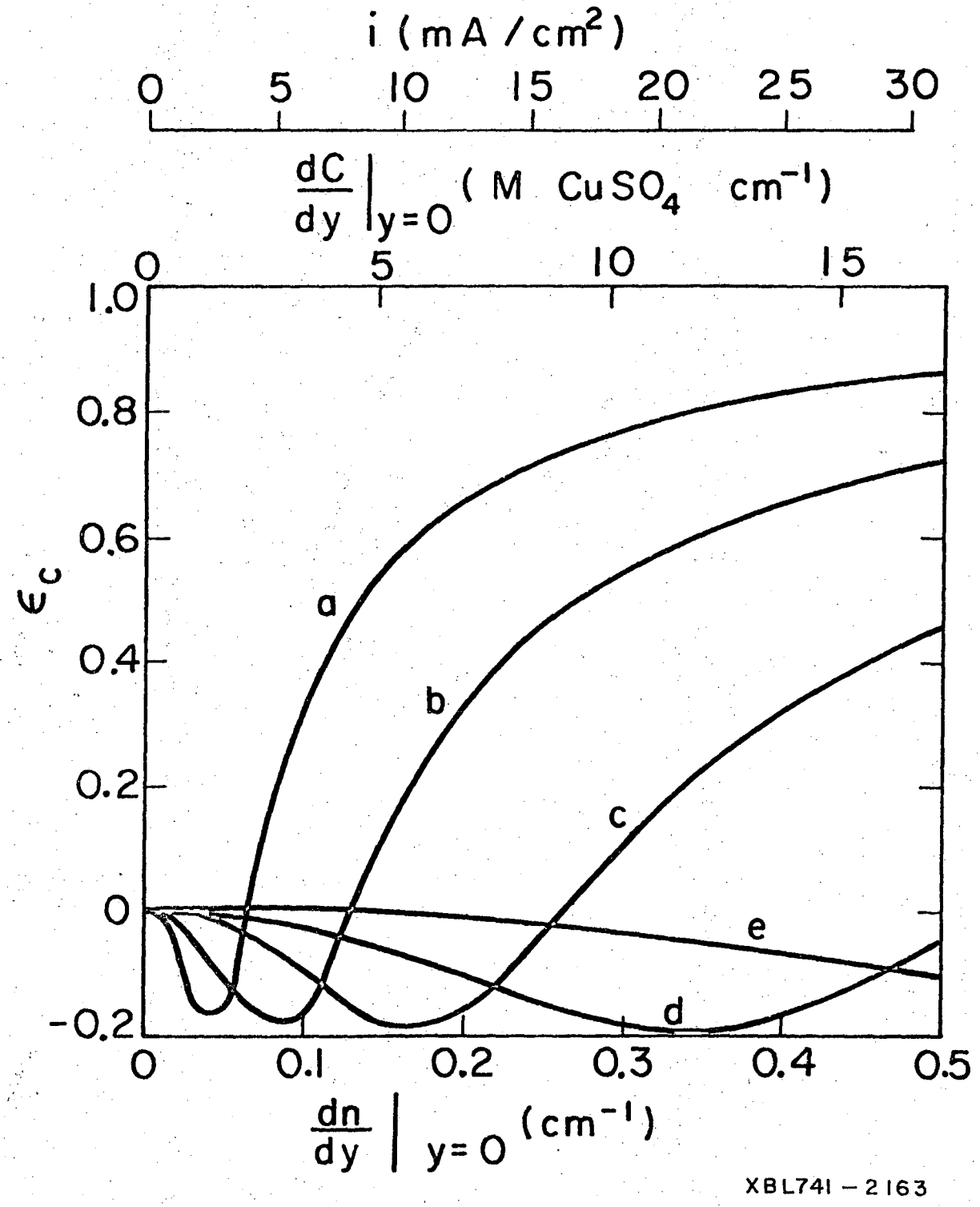
i (mA/cm²)
0
5
10
15
20
25
30
dC/dy |y=0 (M CuSO4 cm⁻¹)
0
5
10
15
1.0
0.8
0.6
0.4
0.2
0
-0.2
εc
a
b
c
d
e
0
0.1
0.2
0.3
0.4
0.5
dn/dy | y=0 (cm⁻¹)
XBL741-2163

Fig. 12

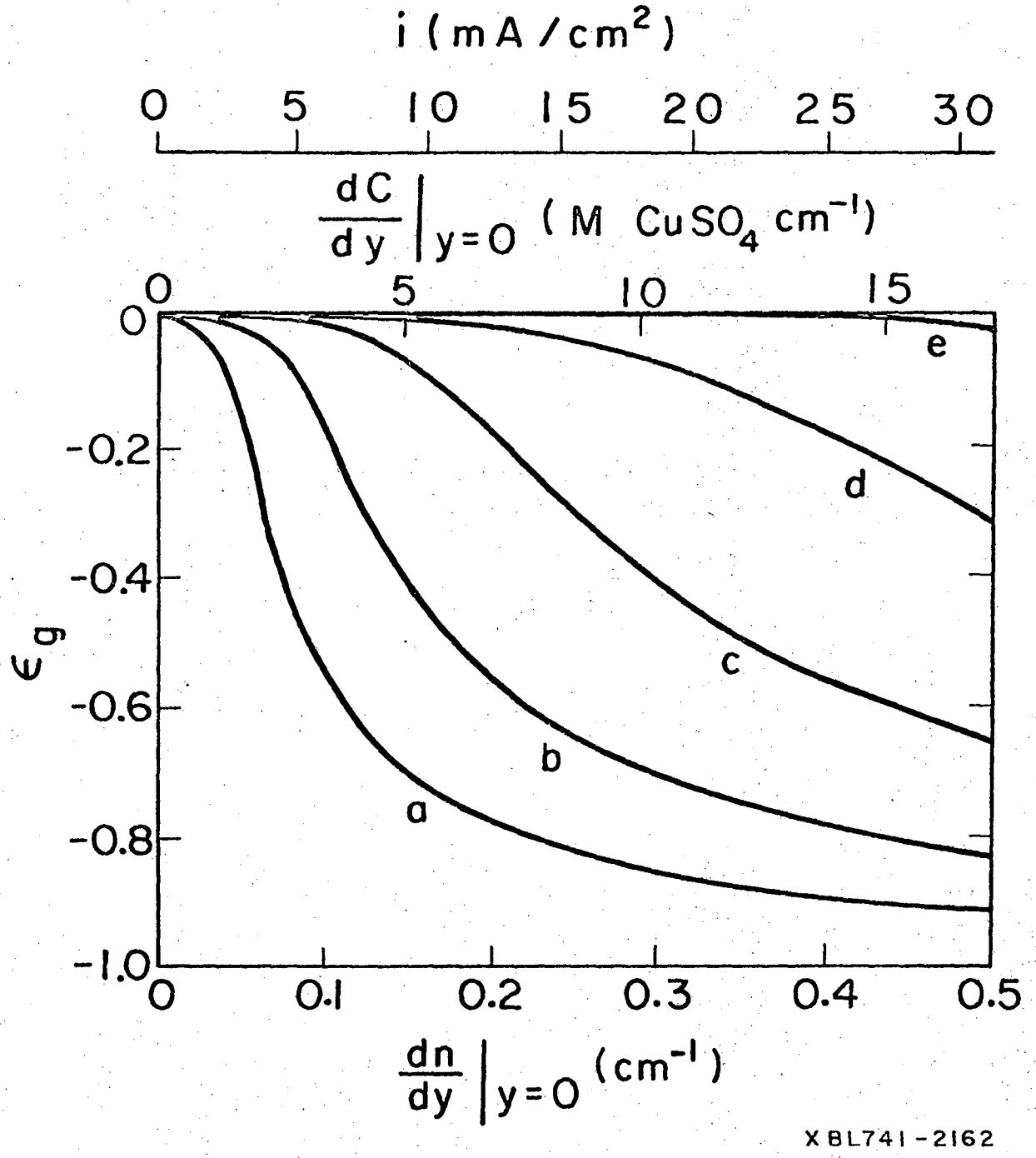
i (mA/cm²)
0
5
10
15
20
25
30
dC/dy |y=0 (M CuSO4 cm⁻¹)
0
5
10
15
0
-0.2
-0.4
-0.6
-0.8
-1.0
εg
a
b
c
d
e
0
0.1
0.2
0.3
0.4
0.5
dn/dy |y=0 (cm⁻¹)
XBL741-2162

Fig. 13

TECHNICAL INFORMATION DIVISION
LAWRENCE BERKELEY LABORATORY
UNIVERSITY OF CALIFORNIA
BERKELEY, CALIFORNIA 94720